ZnO Nanorods Grown on ZnO Sol-Gel Seed Films: Characteristics and Optical Gas Sensing Properties

M. Cittadini,[1] M. Sturaro,[1] M. Guglielmi,[1] A. Resmini,[2] U. Anselmi-Tamburini,[2] P. Koshy,[3] C.C. Sorrell,[3] A. Martucci[1]

[1] Dipartimento di Ingegneria Industriale
Università di Padova
Via Marzolo 9
35131 Padova
Italy

[2] Università di Pavia
Dipartimento di Chimica
V.le Taramelli, 16, 27100 Pavia
Italy

[3] School of Materials Science and Engineering
University of New South Wales
Sydney, NSW 2052
Australia

Corresponding Author: alex.martucci@unipd.it

Keywords: ZnO sol-gel films, ZnO nanorods, Pt nanoparticles, optical gas sensors

Abstract

ZnO sol-gel films, with and without embedded Pt nanoparticles, were used as seeding layers for the hydrothermal growth of ZnO nanorods. The morphology of the nanorods was controlled by adjusting chemicals, concentrations and parameters yielding samples with high transparencies and exposed surface areas. The prepared samples as optical gas sensors were assessed for performance in terms absorbance variation and response time and these data were correlated with the structural properties. The nanorods grown on ZnO films containing Pt nanoparticles showed excellent H_2-

sensing properties owing to the high exposed surface areas of the ZnO nanorods and to the catalytic effect the underlying Pt nanoparticles.

1 Introduction

ZnO is a nontoxic material that has many interesting characteristics, including piezoelectricity [1], ferroelectricity [2], and n-type semiconductivity [3,4]. Owing to these properties, ZnO is one of the most widely used oxides in many devices, such as surface acoustic wave devices, gas sensors, piezoelectric devices, and transparent electrodes [5,6]. ZnO also has been examined as a semiconducting material and so currently is attracting significant attention for optoelectronic devices [7,8].

As an *n*-type semiconductor, ZnO has been used extensively as a gas sensing material, especially for reducing gases, such as H_2 and CO [9]. It is known that the sensing mechanism of ZnO is of the surface-controlled type [10], in which the grain sizes, surface states, and oxygen adsorption quantities play important roles in the gas sensitivity. Point defects on ZnO surfaces are extremely important in gas sensing as they produce very large changes in the surface conductivity. These changes occur owing to charge transfer and band bending caused by the adsorbates.

Recently, gas sensors based on ZnO nanowires (NWs) or nanorods (NRs) with improved gas sensing properties have been fabricated [11,12,13,14,15] owing to their high exposed surface areas. Most of the literature on ZnO NRs-based gas sensors deals with conductometric sensors while the only publications on optical gas sensors report datae for the variation in the photoluminescence properties of ZnO NRs in the presence of oxygen [16] or of ZnO nanopods in the presence of humidity [17].

The present work reports seminal data on the characteristics and performance of ZnO NRs as optical gas sensors as a function of variation in their optical absorbance in the presence of reducing gases. The synthesis conditions were used to control the aspect ratio of the ZnO NRs, which was selected to achieve a compromise between surface area and optical transparency. Further, the role of Pt nanoparticles (NPs) as catalyst for gas sensing also was investigated.

2 Experimental Procedure

ZnO sols were prepared using zinc acetate ($Zn(CH_3COO)_2$), ethanol (C_2H_5OH) and monoethanolamine (MEA, $(CH_2CH_2OH)NH_2$) [18]; all raw materials were reagent-grade from Sigma Aldrich. Zinc acetate solution in ethanol (0.5 M) was prepared and MEA was added dropwise with rapid magnetic stirring so as to achieve a Zn/MEA ratio of 1.0 over a period of ~2 min. This mixture then was magnetically stirred for 1 h.

Platinum colloids of ~15 nm of diameter were prepared using the polyol method [19]. In this method, 67 mg of H_2PtCl_6 and 18.7 mg of NaCl were dissolved in 3 mL ethylene glycol, degassed and kept under inert atmosphere. Separately, 150 mg $NaNO_3$ and 55 mg PVP were dissolved into 13 mL ethylene glycol, degassed, and brought at 160°C under inert atmosphere. After 20 minutes, the former solution was quickly injected into the latter: a change in colour from pale orange to brown-black was observed within a few minutes. The Pt colloidal solution was kept at 160°C under nitrogen for 30 minutes, then cooled down to room temperature, precipitated with excess acetone, centrifuged at 4000 rpm for 5 minutes and re-dispersed in ethanol leading to a 30 mM nominal concentration.

In order to provide precursors for sols with identical Zn concentrations but with and without Pt NPs, the ZnO sol was divided in two equal portions. The former was mixed with the Pt sol in ethanol in an amount yielding 5 mol% Pt. The latter was mixed with pure ethanol of the same volume (but without the Pt NPs). Both Pt NPs-loaded and pure ZnO sols were then deposited by spin coating (model, manufacturer) at 3000 rpm for 30 sec on fused SiO_2 substrates or Si substrates (for scanning electron microscopy, SEM, only). The films were dried by heating in air at 100°C for 10 min, inserting directly into an oven pre-heated to 400°C, annealing for 30 min, and removing from the oven. The preceding methods produced ZnO films (*ZnO*) and ZnO films containing Pt NPs (*ZnO Pt*).

Short ZnO NRs were grown through a hydrothermal process by using the ZnO and ZnO Pt sol-gel films as seed layers. 80 mL of an aqueous solution of zinc nitrate hexahydrate ($Zn(NO_3)_2 \cdot 6H_2O$) and hexamethylenetetramine (HMT) 10 mM equimolar were firstly prepared in a Teflon vessel. ZnO and Pt-loaded ZnO seed layers obtained as described above were placed then into the vessel, leaning on the walls with an angle of about 30 ° and facing the bottom of the vessel to prevent the deposition of precipitate onto the film-side. The vessel was subsequently placed in a hydrothermal reactor (Parr 4748; Parr Instruments, Moline, IL, USA) and the whole assemply held at 60°C for 18 h in an oven. Finally, short NRs-coated ZnO and Pt-loaded ZnO films were then extracted, rinsed

with distilled water, and air-dried. Samples of longer ZnO NRs with length up to 14 μm and aspect ratio above 120 were also prepared on Pt-free ZnO seed layers by using an aqueous solution of zinc nitrate 25 mM, HMT 25 mM, ammonia 650 mM, polyethyleneimine 2.24 mM, at 90 °C and for a soaking time of up to 7h. The soak time was used to control the lengths of the longer NRs while different synthetic conditions were used for the short NRs and the resultant samples, which consisted of substrate, ZnO sol-gel layer, and ZnO NRs, yielding gas sensors with Pt NPs embedded in the ZnO sol-gel layer (*ZnO Pt NR*) and those without Pt NPs (*ZnO NR*).

Optical absorption spectra were obtained in the 200-900 nm wavelength range using a UV-Vis dual-beam spectrophotometer (V 570, Jasco). The haze index, which is the ratio between the total transmittance and the forward scattering out of the normal, was determined using an integrating sphere. The total transmittance was obtained at a 4° incidence angle.

Preferred orientation of the NRs was assessed using glancing angle X-ray diffraction (GAXRD; PW1710 diffractometer, Philips), using a 3° incidence and CuKα radiation at 30 kV and 40 mA.

The microstructures were examined using field emission scanning electron microscopy (FESEM; Tescan Mira 3 XMU, operated at 30 kV. The samples were gold-coated. Analysis of top-view and cross-section FESEM images of the different samples were performed by using ImageJ software. A minimum number of 150 NRs were manually measured in length and diameter to obtain average length, diameter and aspect ratio for each investigated film. A minimum area of 1 μm^2 was then considered to calculate the packing density and the exposed surface area of NRs. All morphological data are summarized in Table 1.

Optical gas sensing tests were performed with optical absorption measurements in the 200-900 nm wavelength range using a Harrick gas flow cell (with 5.5 cm path length) coupled with a Jasco V-650 spectrophotometer. The substrate dimensions were reduced to 10 mm × 20 mm by scoring the substrate and breaking. The standard operating temperature (OT) was set at 300°C and gases at concentrations of 1 vol% CO or H_2 in dry air at a flow rate of 0.4 L/min were used. The incident spectrophotometer beam was normal to the film surface and illuminated an area of 9 mm × 1.5 mm. The adsorption time was defined as the time required to reach 90% of the total response and the desorption time was defined as the time required to reach 90% recovery of the baseline.

3 Results and Discussion

Structural and Optical Properties

Representative haze index [20] measurements were obtained in order to assess the effects of fibre morphology on visible light scattering. These data are summarized in Table 1 and the haze index data are plotted in Figure 1. The principal morphological variable was the NR length, which was controlled by varying the synthesis conditions, as previously described. The overall effect to the eye can be described in terms of the light transmission, where the long ZnO NRs were opaque and the short ZnO NRs were slightly translucent; both were white. Consequently, all data were obtained for samples with short ZnO NRs.

Table 1. Morphological and light scattering data for samples with short and long NRs determined from SEM and haze index data, respectively.

Sample	Average Length (nm)	Average Diameter[A] (nm)	Aspect Ratio (–)	Packing Density (NRs/μm^2)	Surface Area (nm^2/μm^2)	Haze Index at 395 nm (%)
ZnO NR short	370	50	7.4	117	6.5 x 10^6	28
ZnO Pt NR short	280	44	6.4	125	4.6 x 10^6	?
ZnO NR long	14,185	110	129	13	6 x 10^7	79

[A] Distance between parallel faces

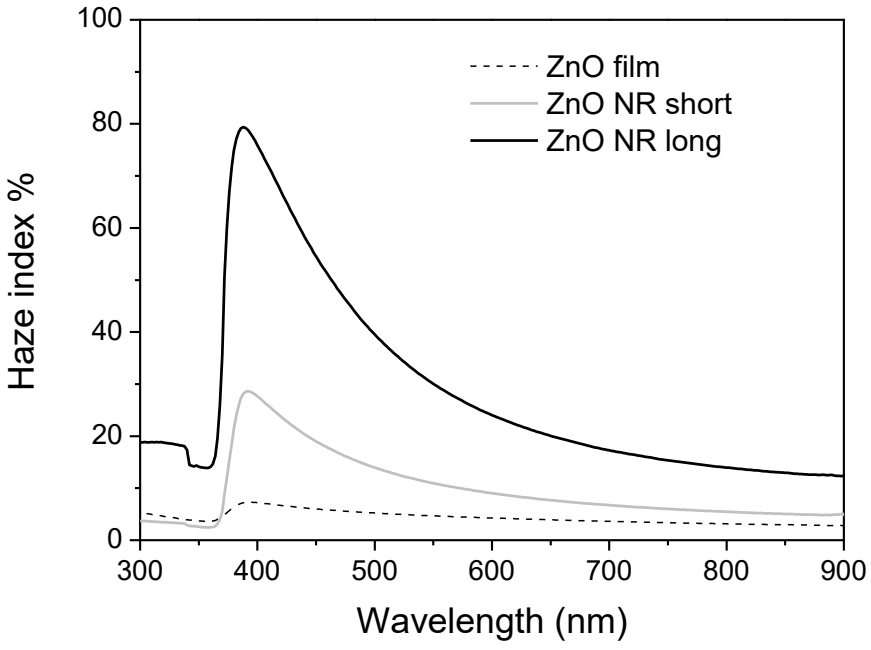

Figure 1. Effects of NR lengths on haze indices for ZnO films and ZnO NR samples.

Representative UV-Vis absorption spectra for the four different samples are given in Figure 2. It can be seen that there is an increase in absorbance for both ZnO and ZnO Pt samples when the NRs are present, reasonably due to their scattering properties. There is also a slight red-shift in the band-edge absorption, which indicates that the ZnO NRs have a smaller band-gap compared to ZnO sol-gel film, as reported previously [21,22]. Furthermore, it also can be seen that there is a significant increase in the degree of scattering when Pt is embedded, which is associated with the strong UV absorption by Pt [23] and, to a lesser extent, the extra interfaces between Pt and ZnO, which have different refractive indices.

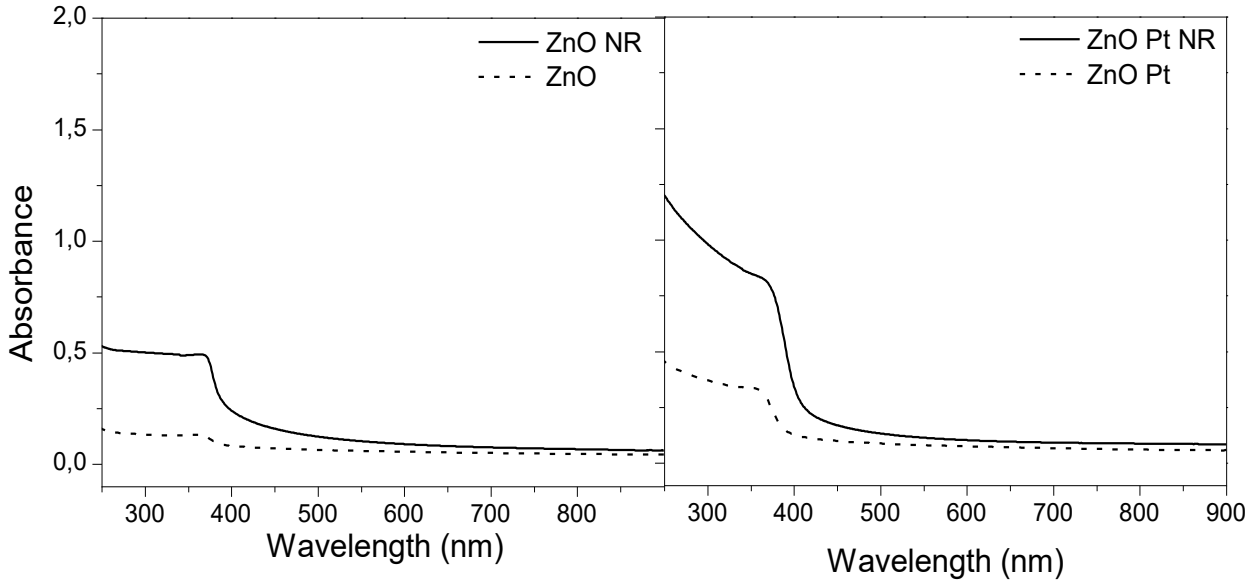

Figure 2. Effects of NRs and Pt on optical absorbance spectra for ZnO films and ZnO NR samples.

Figure 3 shows representative GAXRD patterns for ZnO films and ZnO NR samples. All patterns showed well defined peaks of the würtzite ZnO polymorph; samples with Pt also clearly indicated its presence. XRD pattern of ZnO NR clearly shows a preferred crystalline orientation along (002) accounting for the preferential growth of nanorods along [001] direction, as previously reported in literature for similar samples. [24]. ZnO Pt NR samples did not show any particular changes, indicating that the presence of Pt had no significant effect on the nucleation and growth of the NRs.

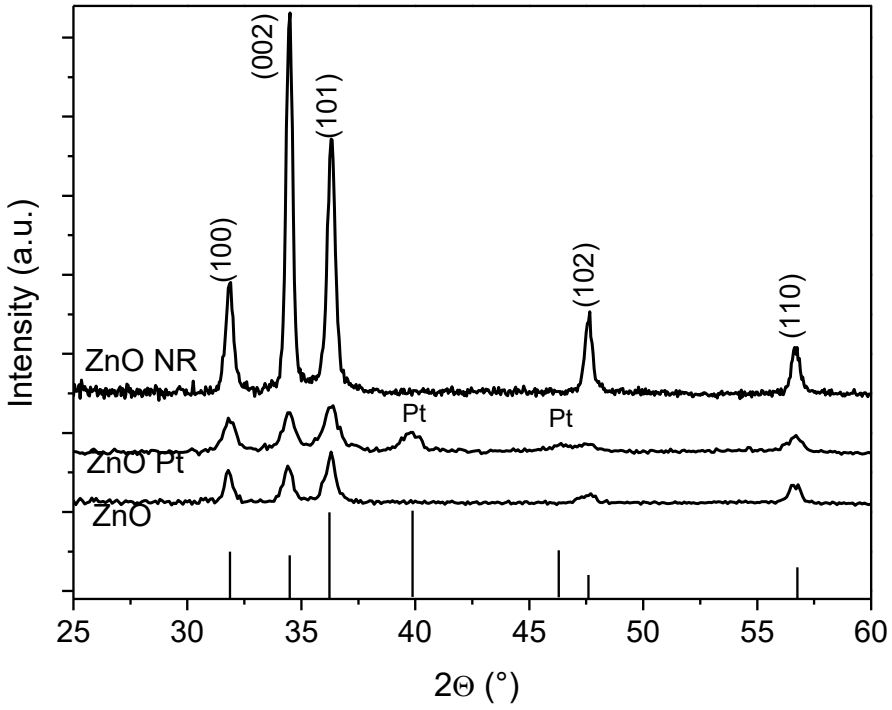

Figure 3. Reported XRD peak intensities for ZnO and ZnO Pt and ZnO NR. Standard patterns on base: ZnO (JCPDS No. 36-1451) and Pt (JCPDS No. 04-0802).

The mean crystallite sizes of the ZnO in the ZnO films and samples were calculated from the line broadening of the diffraction peaks using the Scherrer equation [25] and the grain sizes were estimated from the SEM images; these data are given in Table 2. These data indicate the following:

- There is a slight increase in crystallite size when the ZnO NRs grow from the underlying film, which indicates only minor grain growth.
- This is paralleled in the grain sizes, which also show only a slight increase.
- There appear to be two crystallites per nanorod, so the NRs contain a subgrain boundary, which is known to affect the surface properties [Pham].
- The presence of Pt in the ZnO film caused decreases in the crystallite and grain sizes. Since previous work [23] has shown that Pt is well and densely distributed throughout the microstructure, then size reduction from grain boundary pinning during annealing at 400°C and/or decrease in ZnO areal extent probably are responsible.
- The reduction in size from the Pt effectively reduced the grain size to a single crystallite, thereby eliminating any effects from a subgrain boundary.

Table 2. Mean crystallite size calculated using the Scherrer equation [25], using the full width at half maximum (FWHM) of the diffraction peaks shown in Figure 3.

Sample	Crystallite Size (nm)		Grain Size (nm)	
	ZnO	**Pt**	**ZnO**[A]	**Pt**[B]
ZnO	26	–	30	–
ZnO NR	32	–	50	–
ZnO Pt	20	15	20	–
ZnO Pt NR	23	15	44	–

[A] Grain size of NRs = Distance between parallel faces (Table 1)

[B] Pt grain size could not be determined owing to the Au coating

Figure 4 shows representative FESEM images of the samples with and without Pt. The sol-gel films (Figure 4a) show a homogeneous distribution of fine ZnO grains; the effect of Pt on grain size reduction is clear. The nanorods (Figure 4b) consist of well defined hexagonal elongated grains of relatively consistent diameter (*i.e.*, distance across parallel faces). The morphological data are given in Table 1. The cross-sections (Figure 4c) indicate that the ZnO films are <100 nm in thickness and they confirm that the grain sizes in the ZnO films are less those of the NRs and that Pt suppresses ZnO grain growth. It is important to note that, when the NR length, diameter, and packing density (Table 1) are considered, the surface areas available at the gas-solid interface for the NRs with and without Pt are approximately the same.

Figures go here

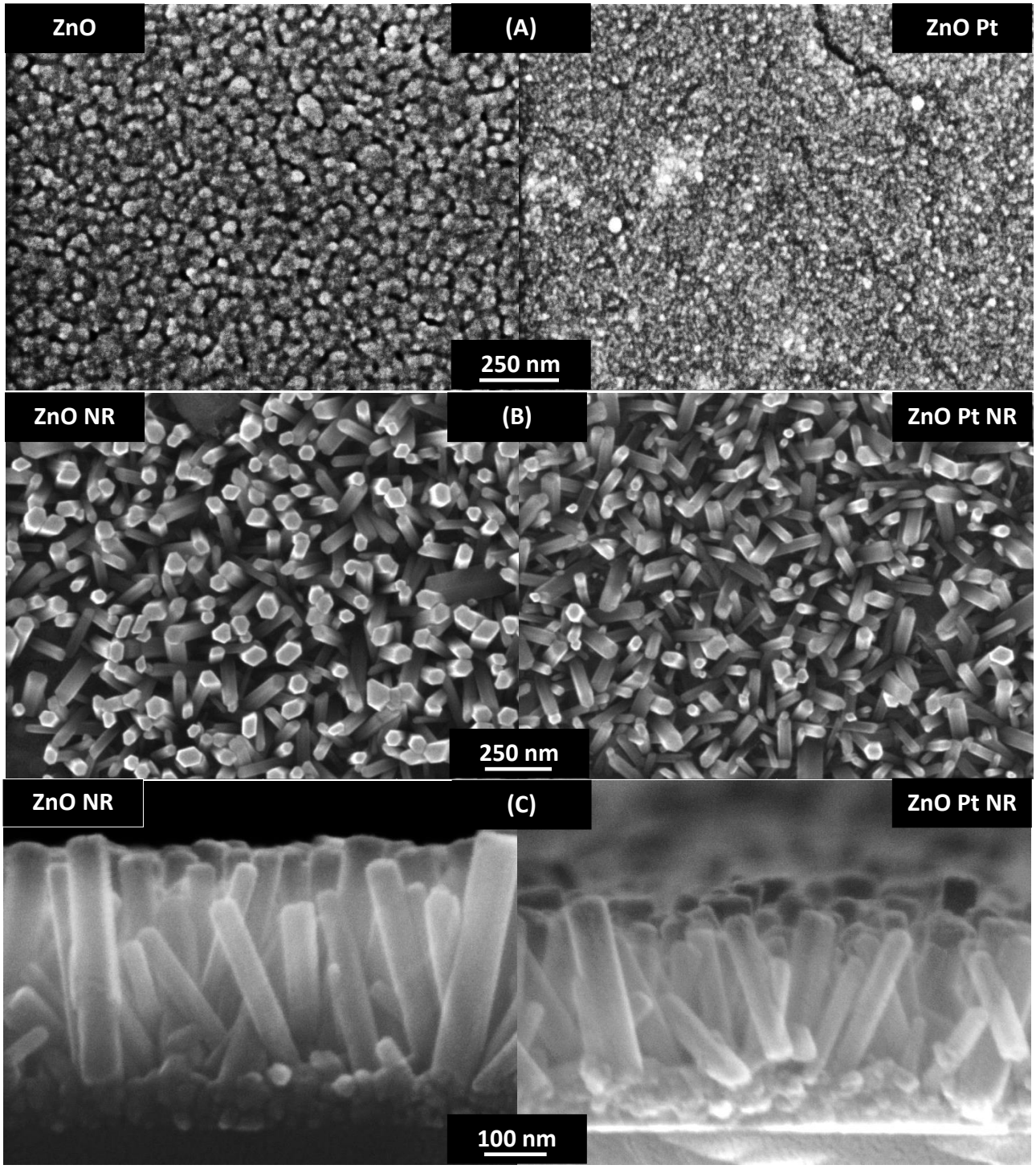

Figure 4 a. FESEM images of ZnO (left) and ZnO Pt (right) sol-gel films. **b.** FESEM images of ZnO NR (left) and ZnO Pt NR (right) samples. **c.** FESEM images of cross-sections of ZnO NR (left) and ZnO Pt NR (right) samples

The laser Raman microspectroscopy patterns are given in Figure 5. Most of the peaks are assigned to fused silica, with the single key peak from wurtzite at 437 cm^{-1} is indicative of würtzite [26]. It is probable that the peak heights are consistent with the effect of the morphology on the degree of

vibration. That is, as given in Table 1, the largest peak corresponds to sample ZnO NR (370 nm NR length), the smaller peak corresponds to sample ZnO Pt NR (240 nm NR length), and the minute peak corresponds to sample ZnO (no NRs); sample ZnO Pt showed no peak. These data are consistent with the view that the peak height is proportional to the amount of material and/or inversely proportional to the degree of damping. That is, the amount of ZnO is minimal but the damping is greatest when the ZnO is isotropic and anchored to the substrate while the samples with NRs have increasing volumes and are able to vibrate in proportion to their lengths. It is possible that Pt also plays a role in damping, although this is considered unlikely since these grains are located at the bases and hence the anchor-points of the NRs.

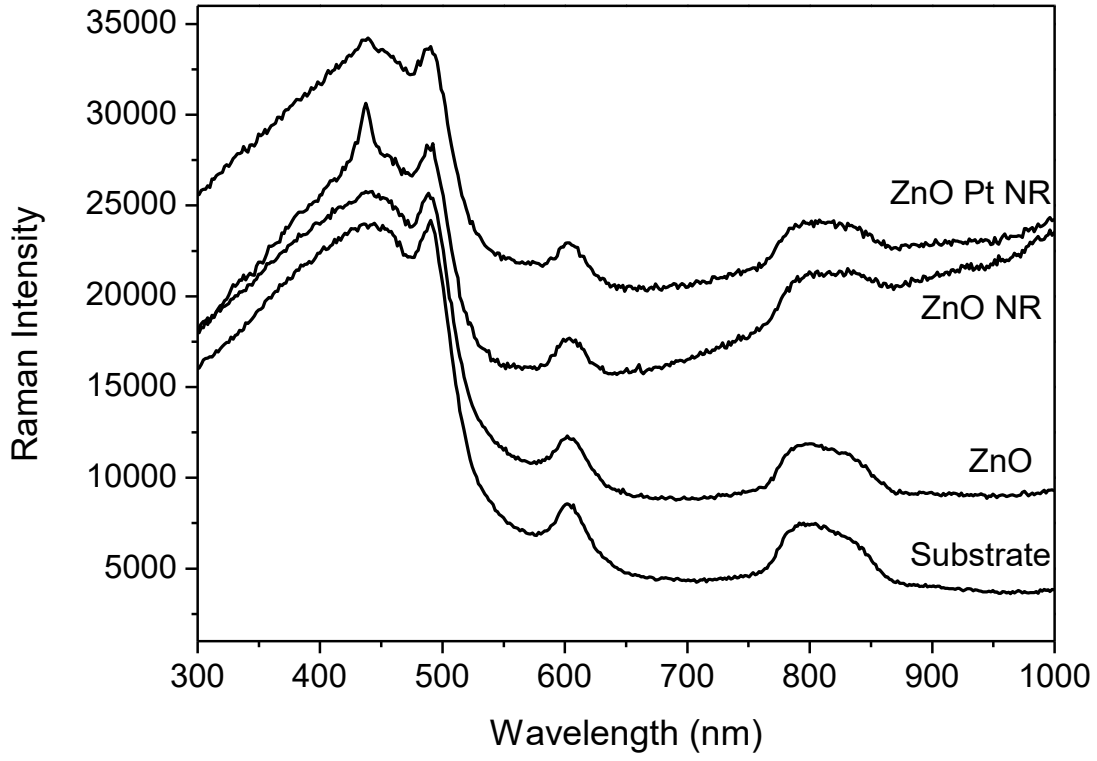

Figure 5. Laser Raman microspectra of fused silica substrate, ZnO film, ZnO NR sample, and ZnO Pt NR sample.

Figure 6 shows the representative photoluminescence (PL) data for a ZnO film. These data indicate that the spectrum is dominated the broad emission centered at ~620 nm from the ZnO defect state [27]. The nature of these intrinsic and/or extrinsic defects is unclear as the literature is not consistent [27]. Other data (not shown) demonstrate that the small emission at ~760 nm is from the fused silica substrate. There also is a weak emission in the UV range (~380 nm) associated with the

band gap (insert) [27]. Although PL data for a ZnO NR sample were obtained, they were similar to those for the ZnO film, albeit with more intense emissions (and noisier).

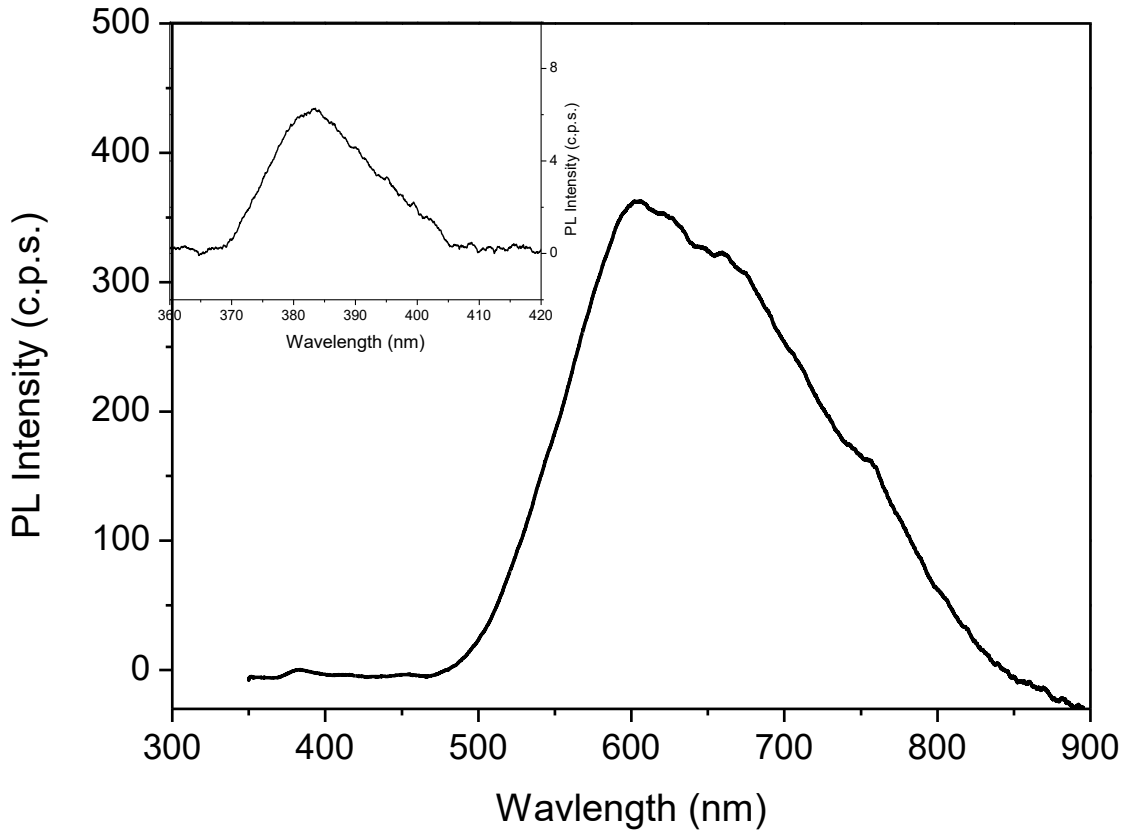

Figure 6. Photoluminescence spectra of ZnO film (excitation at 325 nm); inset shows enlargement of peak (~380 nm) from the band gap.

Gas Sensing Properties

The optical gas sensing properties were evaluated by measuring the variation in the optical absorbance in the presence of H_2 or CO at an OT of 300°C. In order to assess the variation in the absorbance in the presence of the target gas and to compare the optical gas sensing performances of the different samples, an Optical Absorbance Change (OAC) parameter, which is defined as the difference between the absorbance in air and the absorbance during gas exposure (*viz.*, OAC = $Abs_{Air} - Abs_{Gas}$), was used.

Figure 7 showd the absorption spectra of the ZnO Pt NR sample in air and H_2 and Figure 8 shows the OAC for H_2 exposure for the ZnO NR and the ZnO Pt NR samples. The major variation in the absorbance is located in the band-gap region (*i.e.*, 320-420 nm) owing to a blue shift in the optical direct band gap caused by H_2, which is a reducing gas. The blue shift is emphasized in the OAC

curve, shown in Figure 8, by a negative peak centered at ~390 nm; this is particularly evident for the ZnO Pt NR sample.

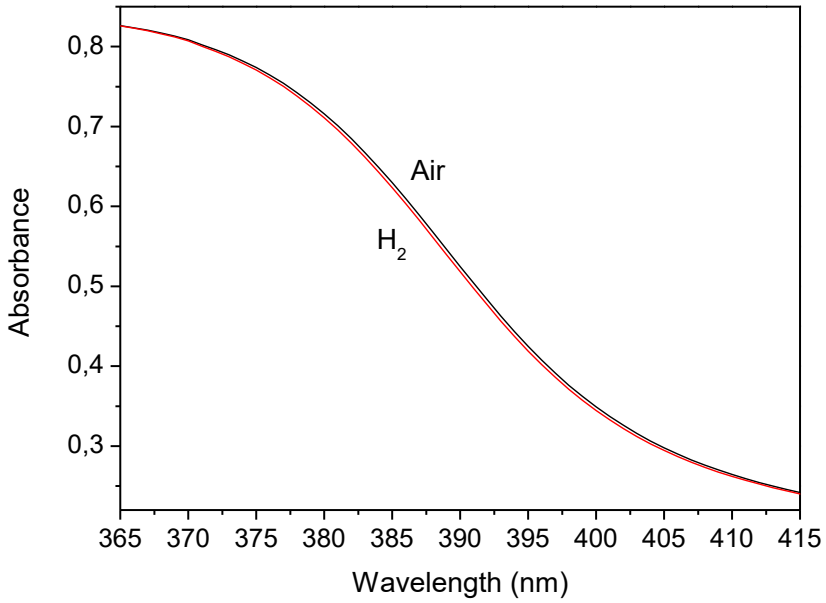

Figure 7. Absorbance spectra of ZnO Pt NR in air and H_2.

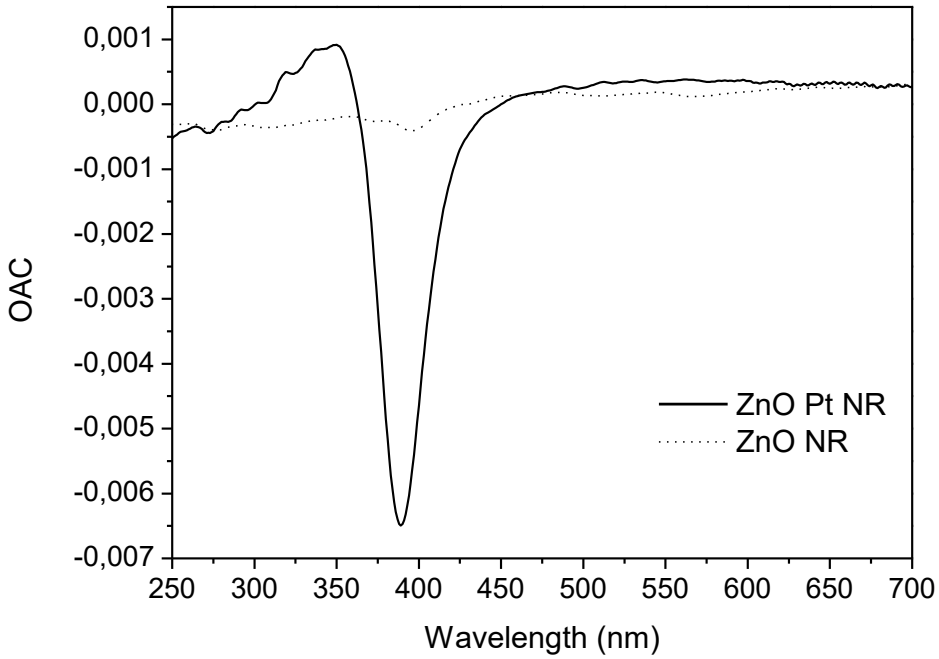

Figure 8. OAC for H_2 exposure for the samples ZnO NR and ZnO Pt NR.

The interaction of reducing gases with transition metal oxides, especially ZnO, has been investigate extensively [9,28]. ZnO (n-type) typically is characterized by the occurrence of oxygen vacancies (*viz.*, ZnO_{1-x}) [29]. Atmospheric oxygen has been reported to adsorb preferentially at the surface defects of ZnO, forming O_2^-, O^-, and $O^=$, and resulting in changes in the electrical conductivity and

optical properties [30]. Previous studies on the adsorption of oxygen on metal oxides have highlighted the observation that the stable oxygen ions are O_2^- at <100°C, O^- at 100°-300°C, and $O^=$ at >300°C [31,32].

Since the samples were tested in dry air as optical sensors at the OT of 300°C, it is probable that adsorbed oxygen dominates and include the following general adsorption reactions:

$$\tfrac{1}{2}O_2 + e^-_{(cb)} \rightarrow O^-_{(ads)} \quad (1)$$

$$\tfrac{1}{2}O_2 + 2e^-_{(cb)} \rightarrow O^=_{(ads)} \quad (2)$$

where *cb* and *ads* represent *conduction band* and *adsorbed*, respectively.

The possible interactions of reducing gases (CO, H_2) with of the metal oxide are expected to be as follows:

$$CO + O^-_{(ads)} \rightarrow CO_2 + e^-_{(cb)} \quad (3)$$

$$CO + O^=_{(ads)} \rightarrow CO_2 + 2e^-_{(cb)} \quad (4)$$

$$H_2 + O^-_{(ads)} \rightarrow H_2O + e^-_{(cb)} \quad (5)$$

$$H_2 + O^=_{(ads)} \rightarrow H_2O + 2e^-_{(cb)} \quad (6)$$

Consequently, interaction of the reducing gases with ZnO_{1-x} is expected to increase the concentration of electrons in the conduction band, which induces an increase in the band gap (*i.e.*, *Burstein-Moss effect* [33,34]) and is confirmed by the blue-shift indicated in Figures 7 and 8.

The OAC curves shown in Figure 8 demonstrate that the ZnO Pt NR samples show a stronger response compared to that of the ZnO NR samples. This effect is attributed to the catalytic effect of Pt for hydrogen oxidation [35,36]. It may be noted that this effect is significant even though the Pt NPs are embedded in the ZnO film underlying the ZnO NRs, which probably is facilitated by the high mobility of H_2 molecules at 300°C [37].

Dynamic absorbance tests were conducted at the fixed wavelength range of 390-400 nm, where the change in absorbance was the highest, as shown Figure 8. The significant effects of Pt and NRs for an air-H_2-air cycle are shown in Figures 9 and 10, respectively.

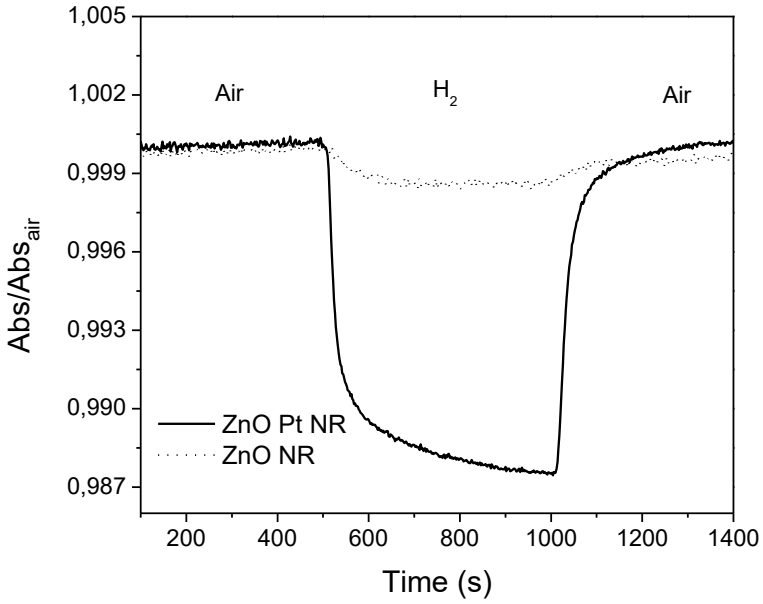

Figure 9. Variation in absorbance at 390 nm for an air-H_2-air cycle.

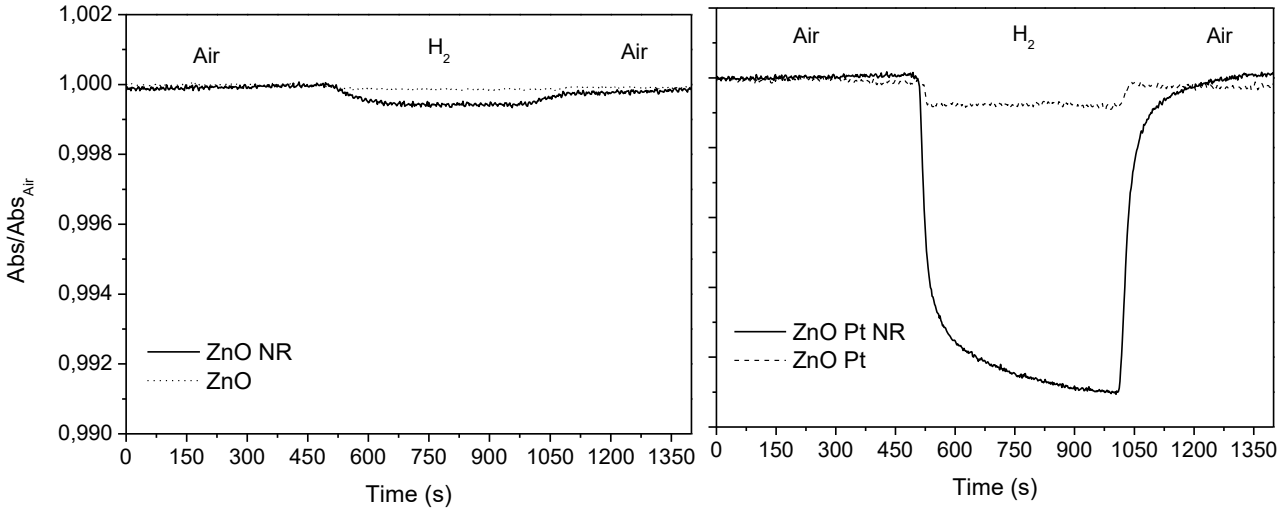

Figure 10. Variation in absorbance at 390 nm for an air-H_2-air cycle.

Both ZnO NR and ZnO Pt NR samples showed a significantly higher variations in the absorbance relative to those of the ZnO and ZnO Pt samples, respectively. The gas-sensing properties of ZnO NRs are controlled princaipally by their surfaces and are controlled by one of two different mechanisms, depending on the diameter and length of the rod: contact-controlled or surface-depletion-controlled [38].

Contact-controlled sensing is typical of rods with diameters of 10^2 nm and lengths up in the low-μm range, as in the present case. Surface-depletion-controlled sensing is dominant with rods of diameter <15 nm and lengths <1 μm of length, where the diameter of the rod is comparable to the

width of the depletion layer [37]. Hence, the superior gas-sensing performances of the samples with NRs are explained by the greater exposed surface areas relative to those of the ZnO films. It also may be noted that the exposed surface areas of the NRs of both the ZnO NR and ZnO Pt NR samples are of the same order of magnitude, as shown in Table 1, which highlights the effect of Pt.

The samples also were tested as CO gas sensors but only samples with Pt NPs gave detectable signals. Figure 11 shows the variation in the absorbance at 400 nm for an air-CO-air cycle. Although the signal was relatively small, the catalytic effect of the Pt NPs for the CO sensing is clear.

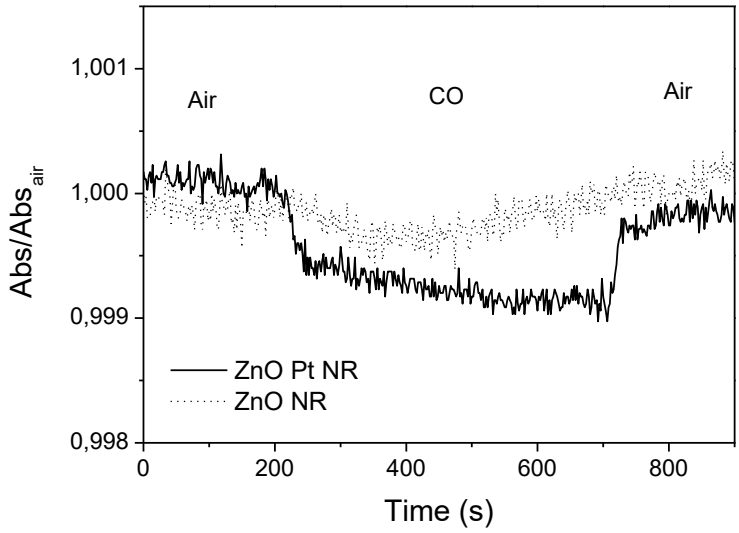

Figure 11. Variation in absorbance at 400 nm for an air-CO-air cycle.

Prolonged time-resolved gas-sensing measuremnts are shown in Figure 12. The reversible dynamic response to H_2, with almost complete recovery of the baseline level, clear responses, and short recovery times, is apparent, although the response to CO is poorly defined. The response times for H_2, sample thicknesses, and maximal optical absorption variations (ΔA_{Max}) are given in Table 3. These data indicate that the presence of Pt NPs not only increases the ΔA_{Max} (for both ZnO films and ZnO NR samples) but also decreases both the adsorption and desorption times. As discussed, the presence of NRs increases of the ΔA_{Max} owing to the greater exposed surface area. The NRs also increase the number of species adsorbed (O^-, $O^=$) that can react with the gas molecules and increase the efficiency of the electron injection into the ZnO matrix.

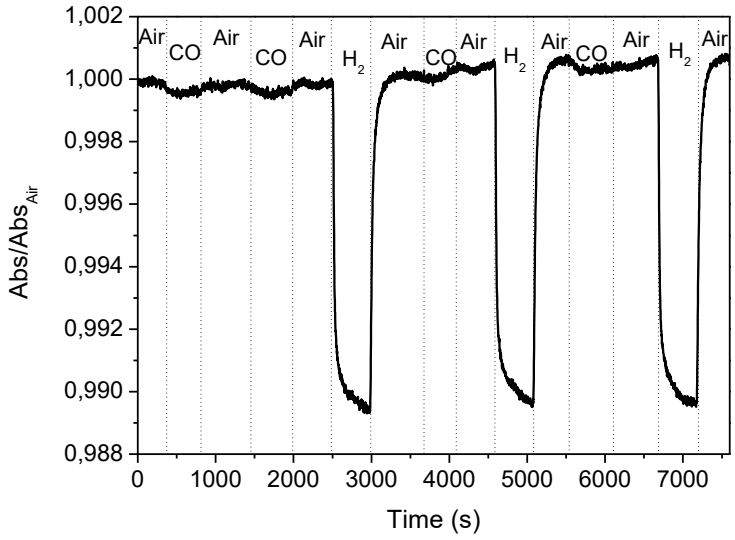

Figure 12. Time-resolved measurements of absorption change for ZnO Pt NR at 400 nm.

In light of the response times given in Table 3, the presence of NRs appears to induce a general increase in the response time, which is very clear for desorption and for Pt. This is likely to result from the greater thickness and associated exposed surface area of the samples with NRs. In fact, comparison of the curves for the absorbance data (*e.g.*, Figure 10) for the ZnO films and ZnO NR samples during desorption shows that, at the 90% ΔA_{Max} level for the ZnO film, the same absolute absorbance variations are achieved at ~60 s for the ZnO film but only at ~5 s for the ZnO NR sample.

Table 3. Adsorption and desorption times for H_2, thickness, and maximal optical absorption variation.

Sample	Adsorption Time (s)	Desorption Time (s)	Thickness (nm)	Maximal Absorption Variation (‰)
ZnO	120±15	60±5	<100	0.2
ZnO NR	110±15	90±8	~500	0.6
ZnO Pt	40±5	40±5	<100	0.8
ZnO Pt NR	70±5	90±5	~400	5.2

4 Conclusions

ZnO NRs have been grown successfully on ZnO sol-gel films. The length of the NRs was controlled in order to produce samples with relatively high optical transparencies and exposed

surface areas for optical gas sensors. Their presence and morphology greatly improve the gas-sensing properties in terms of both sensitivity and response time owing to the high exposed surface areas and hence the areal density of the interaction sites. The presence of Pt NPs in the underlying ZnO film greatly enhances the gas-sensing properties of the NRs owing to the catalytic effect of Pt for hydrogen oxidation. The combination of the high surface area of the NRs and the catalytic effect of the Pt NPs indicates that the ZnO Pt NR samples are suitable as H_2 optical sensors with high sensitivities.

Acknowledgments

This work was supported by Italian PRIN_09 Project N° 2009ALAX7Y "Sviluppo di materiali con architettura gerarchica per sensori di ossidi di azoto a bassa temperatura per il monitoraggio ambientale". A. Martucci wishes to thanks University of New South Wales for supporting him through the Faculty of Science Visiting Research Fellowship.

References

[1] Young Hwan Hwang, Seok-Jun Seo, and Byeong-Soo Bae J. Mater. Res., Vol. 25, n° 4, 695 (2010).

[2] J.G.E. Gardeniers, Z.M. Rittersma, and G.J. Burger, J. Appl. Phys. 83, 7844 (1998).

[3] Dhananjay, J. Nagaraju, and S.B. Krupanidhi, J. Appl. Phys. 99, 034105 (2006).

[4] V. Bhosle, A. Tiwari, and J. Narayan, J. Appl. Phys. 100, 033713 (2006).

[5] U. Ozgur, Ya.I. Alivov, C. Liu, A. Teke, M.A. Reshchikov, S. Dogan, V. Avrutin, S. Cho, and H. Morkoc, J. Appl. Phys. 98, 041301 (2005).

[6] C. Woll: The chemistry and physics of zinc oxide surfaces. Prog. Surf. Sci. 82, 55 (2007).

[7] E. Fortunato, P. Barquinha, A. Pimentel, A. Goncalves, A.Marques, L. Pereira, and R. Martins, Thin Solid Films 487, 205 (2005).

[8] B.S. Ong, C. Li, Y. Li, Y. Wu, and R. Loutfy, J. Am. Chem. Soc. 129, 2750 (2007).

[9] G. Eranna, B. C. Joshi, D. P. Runthala, R. P. Gupta, Oxide Materials for Development of Integrated Gas Sensors—A Comprehensive Review Critical Reviews in Solid State and Materials Sciences, 29:111–188, 2004.

[10] Gergintschew, Z.; Fo¨rster, H.; Kositza, J.; Schipanski, D. *Sens. Actuators, B* **1995**, *26-27*, 170.

[11] K.V. Gurav, P.R. Deshmukh, C.D. Lokhande, LPG sensing properties of Pd sensitized vertically aligned ZnO nanorods, Sens. Actuators B 151 (2011) 365–369.

[12] L. Liao, H.B. Lu, J.C. Li, H. He, D.F. Wang, D.J. Fu, C. Liu, W.F. Zhang, Size dependence of gas sensitivity of ZnO nanorods, J. Phys. Chem. C 111 (2007) 1900–1903.

[13] J. Xu, Y. Zhang, Y. Chen, Q. Xiang, Q. Pan, L. Shi, Uniform ZnO nanorods can be used to improve the response of ZnO gas sensor, Mater. Sci. Eng. B 150 (2008) 55–60.

[14] J. Yi, J.M. Lee, W.I. Park, Vertically aligned ZnO nanorods and graphene hybrid architectures for high-sensitive flexible gas sensor, Sens. Actuators B 155 (2011) 264–269.

[15] K.V. Gurav, M.G. Gang, S.W. Shin, U.M. Patil , P.R. Deshmukh, G.L. Agawane, M.P. Suryawanshi, S.M. Pawar, P.S. Patil , C.D. Lokhande, J.H. Kim, Gas sensing properties of hydrothermally grown ZnO nanorods with different aspect ratios, Sensors and Actuators B 190 (2014) 439– 445.

[16] J.R. Sanchez-Valencia, M. Alcaire, P. Romero-Gómez, M. Macias-Montero, F. J. Aparicio, A. Borras, A. R. Gonzalez-Elipe, A. Barranco, Oxygen Optical Sensing in Gas and Liquids with Nanostructured ZnO Thin Films Based on Exciton Emission Detection, J. Phys. Chem. C 2014, 118, 9852−9859

[17] R. Majithia, S. Ritter, K.E. Meissner, Heterogeneous nucleation for synthesis of sub-20 nm ZnO nanopodsand their application to optical humidity sensing, Analytica Chimica Acta 812 (2014) 206– 214

[18] E. Della Gaspera, M. Guglielmia, A. Martucci, L. Giancaterini, C. Cantalini, Enhanced optical and electrical gas sensing response of sol–gel based NiO–Au and ZnO–Au nanostructured thin films Sensors and Actuators B 164 (2012) 54– 63

[19] T. Herricks, J. Chen, Y. Xia, "Polyol Synthesis of Platinum Nanoparticles: Control of Morphology with Sodium Nitrate", *Nano Letters*, Vol. 4, pp. 2367–2371, 2004.

[20] Designation D 1003-92 American Society for testing and materials.

[21] Magnus Willander, Omer Nur, Siama Zaman, A Zainelabdin, Nargis Bano and I Hussain, Zinc oxide nanorods/polymer hybrid heterojunctions for white light emitting diodes, 2011, JOURNAL OF PHYSICS D-APPLIED PHYSICS, (44), 22, 224017.

[22] L. Znaidi, G.J.A.A. Soler Illia, S. Benyahia, C. Sanchez, A.V. Kanaev, Oriented ZnO thin films synthesis by sol–gel process for laser application Thin Solid Films 428 (2003) 257–262.

[23] E. Della Gaspera, M. Bersani, G. Mattei, T.-L. Nguyen, P. Mulvaney, A. Martucci. *Cooperative effect of Au and Pt inside TiO_2 matrix for optical hydrogen detection at room temperature using surface plasmon spectroscopy* NANOSCALE (2012) 4, 5972-5979.

[24] I. G. Tredici, A. Resmini, F. Yaghmaie, M. Irving, F. Maglia, U. Anselmi-Tamburini, A simple two-step solution chemistry method for synthesis of micropatterned ZnO nanorods based on metal-loaded hydrogels, Thin Solid Films 526 (2012) 22–27.

[25] B.D. Cullity, S.R. Stock, Elements of X-ray diffraction, third ed., Prentice-Hall, New Jersey, 2001.

[26] S. Ben Yahia, L. Znaidi, A. Kanaev, J.P. Petitet, "Raman Study of Oriented ZnO Thin Films Deposited by Sol-Gel Method", *Spectrochimica Acta Part A: Molecular and Biomolecular Spectroscopy*, **71** [4] 1234-38 (2008).

[27]H. Zeng, G. Duan, Y. Li, S. Yang, and X. Xu, "Blue Luminescence of ZnO Nanoparticles Based on Non-Equilibrium Processes: Defect Origins and Emission Controls", *Advanced Functional Materials*, **20** [4] 561-72 (2010).

[28] E. Comini Metal oxide nano-crystals for gas sensing Analytica Chimica Acta 568 (2006) 28–40.

[29] P.Kofstad, Non-Stoichiometric, Diffusion and Electrical Conductivity in binary metal oxides, Wiley, New York, 1972.

[30] M.-W. Ahn, K.-S. Park, J.-H. Heo, J.-G. Park, D.-W. Kim et al., Gas sensing properties of defect-controlled ZnO-nanowire gas sensor, Appl. Phys. Lett. 93, (2008) 263103115.

[31] S.C.Chang, Oxygen chemisorption on tin oxide: correlation between electrical conductivity and EPR measurements, J.Vac.Sci. Technol. 17 (1980) 366 -369.

[32] A.Z.Sadek, S.Choopun, S.J. Ippolito, K.Kalantar-zadeh, Characterization of ZnO nanobelt-based gas sensor for H2, NO2 and Hydrocarbon sensing, IEEE Sens. J., 7 (2007) 919-924.

[33] Melnick, D. A. J. Chem. Phys. 1957, 26, 1136−1146.

[34] Tanaka, K.; Blyholder, G. J. Phys. Chem. 1972, 76, 3184−3187

[35] S. Völkening, K. Bedürftig, K. Jacobi, J. Wintterlin, G. Ertl, *Phys. Rev. Lett.* 1999, **83**, 2672.

[36] M. Andersson, A. Rosén, *J. Chem. Phys.* 2002, **117**, 7051.

[37] Psofogiannakis, Froudakis; J. Phys. Chem. C, 2009, 113 (33), pp 14908–14915.

[38] C. C. Li, Z. F. Du, L. M. Li, H. C. Yu, Q. Wan, T. H. Wang Appl. Phys. Lett. 91, 032101, 2007.